

Giant mechanocaloric materials for solid-state cooling

Junran Zhang(张俊然), Yixuan Xu(徐逸轩), Shihai An(安世海), Ying Sun(孙莹), Xiaodong Li(李晓东), Yanchun Li(李延春)

Citation: Chin. Phys. B . 2020, 29(7): 076202 . **doi:** 10.1088/1674-1056/ab8a40
Journal homepage: http://cpb.iphy.ac.cn; http://iopscience.iop.org/cpb

What follows is a list of articles you may be interested in

Electronic structure and phase transition engineering in NbS_2: Crucial role of van der Waals interactions

Wei Wang(王威), Wen Lei(雷文), Xiaojun Zheng(郑晓军), Huan Li(黎欢), Xin Tang(唐鑫), Xing Ming(明星)

Chin. Phys. B . 2020, 29(5): 056201 . **doi:** 10.1088/1674-1056/ab8214

Structural and electrical transport properties of Dirac-like semimetal $PdSn_4$ under high pressure

Bowen Zhang(张博文), Chao An(安超), Yonghui Zhou(周永惠), Xuliang Chen(陈绪亮), Ying Zhou(周颖), Chunhua Chen(陈春华), Yifang Yuan(袁亦方), Zhaorong Yang(杨昭荣)

Chin. Phys. B . 2019, 28(12): 126202 . **doi:** 10.1088/1674-1056/ab50b3

Shock-induced migration of asymmetry tilt grain boundary in iron bicrystal: A case study of Σ3 [110]

Xueyang Zhang(张学阳), Kun Wang(王昆), Jun Chen(陈军), Wangyu Hu(胡望宇), Wenjun Zhu(祝文军), Shifang Xiao(肖时芳), Huiqiu Deng(邓辉球), Mengqiu Cai(蔡孟秋)

Chin. Phys. B . 2019, 28(12): 126201 . **doi:** 10.1088/1674-1056/ab4f61

High-pressure electrides: From design to synthesis

Biao Wan(万彪), Jingwu Zhang(张静武), Lailei Wu(吴来磊), Huiyang Gou(缑慧阳)

Chin. Phys. B . 2019, 28(10): 106201 . **doi:** 10.1088/1674-1056/ab3f95

Transport properties of topological nodal-line semimetal candidate $CaAs_3$ under hydrostatic pressure

Jing Li(李婧), Ling-Xiao Zhao(赵凌霄), Yi-Yan Wang(王义炎), Xin-Min Wang(王欣敏), Chao-Yang Ma(麻朝阳), Wen-Liang Zhu(朱文亮), Mo-Ran Gao(高默然), Shuai Zhang(张帅), Zhi-An Ren(任治安), Gen-Fu Chen(陈根富)

Chin. Phys. B . 2019, 28(4): 046202 . **doi:** 10.1088/1674-1056/28/4/046202

REVIEW

Giant mechanocaloric materials for solid-state cooling*

Junran Zhang(张俊然)[1,2], Yixuan Xu(徐逸轩)[1,2], Shihai An(安世海)[3], Ying Sun(孙莹)[3], Xiaodong Li(李晓东)[1], and Yanchun Li(李延春)[1,†]

[1] *Multidiscipline Research Center, Institute of High Energy Physics, Chinese Academy of Sciences, Beijing* 100049, *China*

[2] *School of Physical Sciences, University of Chinese Academy of Sciences, Beijing* 100049, *China*

[3] *School of Physical Sciences, Beihang University, Beijing* 100191, *China*

(Received 15 February 202; revised manuscript received 22 March 2020; accepted manuscript online 17 April 2020)

This article reviews the research progress of measurement techniques and materials on the mechanocaloric effect over the past few decades. Mechanocaloric materials can be divided into elastocaloric and barocaloric materials depending on the applied uniaxial stress or hydrostatic pressure. Elastocaloric materials include non-magnetic shape memory alloys, polymers, and rare-earth compounds. Barocaloric materials include magnetic shape memory alloys, ferroelectric ceramics, superionic conductors, and oxyfluorides. The mechanocaloric effects of these classes of materials are systematically compared in terms of the isothermal entropy change and adiabatic temperature change. In addition to the thermal effects, other characteristics closely related to the application of mechanocaloric materials are also summarized. Finally, perspectives for further development of mechanocaloric materials in the solid-state cooling area are discussed.

Keywords: mechanocaloric materials, elastocaloric effect, barocaloric effect, solid-state cooling

PACS: 62.50.–p, 81.40.Vw, 07.20.Mc **DOI:** 10.1088/1674-1056/ab8a40

1. Introduction

Traditional refrigeration technology is represented by air conditioners and refrigerators, with are mainly driven by steam compression and liquid vaporization. The technology could cause ozone depletion and/or greenhouse effects. Because of environmental concerns, research on solid-state cooling as a next-generation refrigeration technology is expanding. Solid-state refrigeration technology is mainly related to three thermal effects that refer to the reversible thermal response of a given material when subjected to changes in an externally applied mechanical, electric, or magnetic field, namely the mechanocaloric effect (MCE), including the elastocaloric effect (ECE) and barocaloric effect (BCE); the electrocaloric effect (eCE); and the magnetocaloric effect (mCE). The advantages of solid-state refrigeration are that it is efficient and clean, with no emissions and easy recycling.

The search for mechanocaloric materials with giant caloric effect has become a major challenge for the development and application of mechanocaloric cooling equipment. Approximately 200 years ago, the mechanocaloric effect was first described by the natural philosopher John Gough.[1] The elastocaloric effect of various materials was reported by Joule in 1859.[2] In the last three decades, many mechanocaloric materials have been discovered. These mechanocaloric materials can be divided into various classes including alloys, magnetic materials, ceramics, organic–inorganic hybrid perovskites, polymers, oxyfluorides, superionic conductors, and plastic crystals. Of the vast array of mechanocaloric materials, which is a good refrigerant? On the basis of research on mechanocaloric materials, we identify the following main requirements that mechanocaloric materials should meet for solid-state cooling application: (i) good cooling efficiency under low pressure, namely, a large and reversible entropy or/and temperature change; (ii) adequate cooling temperature span; (iii) environmentally friendly; (iv) chemically stable with excellent reproducibility of caloric effects; (v) small hysteresis to rapid cooling cycles; (vi) economical for wide applications. These parameters affect the selection of a refrigerant. The temperature and entropy changes are important parameters, which reflect the cooling efficiency of a mechanocaloric material. It is more economical to use a refrigerant with high cooling efficiency. The cooling temperature span is closely related to the relative cooling power (RCP): $\mathrm{RCP} = |\Delta S_{\max}|\delta T_{\mathrm{FWHM}}$, where $\Delta S_{\max}$ is the maximum of entropy changes and is the full width at half maximum (FWHM) of the ΔS *versus* T curves. An appropriate pressure can increase the cooling efficiency for many mechanocaloric materials if it can be achieved and the materials can support it. In addition, some mechanocaloric materials contain toxic elements that may damage the environment. The refrigerant must have good reproducibility for the long-term use. Furthermore, the stability of the refrigerant, including its thermal and chemical stability, must be considered in designing cooling equipment. Hysteresis restrains the work frequency and cooling capacity. Economical mechanocaloric

*Project supported by the National Natural Science Foundation of China (Grant No. 11474280).

†Corresponding author. E-mail: liyc@ihep.ac.cn

© 2020 Chinese Physical Society and IOP Publishing Ltd

materials are beneficial for widespread applications. Although there have been many review papers on solid-state cooling materials,[3–6] a review that summarizes and compares the various mechanocaloric materials from the application viewpoint, especially for recent materials with colossal mechanocaloric effects, is lacking. The present paper aims to introduce measurement methods, summarize recent progress, and discuss further development in this area.

2. Measurement techniques

The two typical quantities used to characterize the MCE are the isothermal entropy change (ΔS) and adiabatic temperature change (ΔT). The measurement methods can be broadly classified into three types: direct, quasi-direct, and indirect methods.[3] Different methods can be used to obtain different values of ΔS and/or ΔT for the same material. For example, indirect methods usually overestimate ΔS, and direct methods usually underestimate ΔT because of heat leakage.

The direct methods are simple and direct with the temperature determined using a thermocouple or non-contact infrared thermometry. The methods require adiabatic condition to obtain an accurate ΔT. When the speed of the external field changes is much faster than the heat exchange rate between the sample and environment, an adiabatic condition can be considered to be achieved. For example, for foil samples exposed to air in elastocaloric experiments, the adiabatic requirement is met if the strain rate is larger than 0.2 s^{-1}.[7] In barocaloric experiments, the temperature change measured by direct methods is usually underestimated because the pressure medium around the samples leads to a heat leak. For direct measurement of isothermal entropy changes, there is currently no suitable device.

For the quasi-direct methods, ΔS can be determined by measuring the heat capacity or heat flux under high pressure. Differential scanning calorimetry (DSC) under high pressure is the most suitable technique for BCE studies of first-order phase transitions. DSC equipment provides hydrostatic pressure, which is generated by gas such as oxygen or nitrogen. For elastocaloric studies, currently, no suitable calorimetric device can work under uniaxial external loads. When a sample is on a heating run in DSC, the specific heat C^{L} of the low-temperature phase can be measured. Then, the temperature increases to the initial temperature of phase transition (T_1). The phase transition occurs, and the specific heat C can be determined. With continuous heating, the temperature reaches the final temperature of phase transition (T_2). The specific heat C^{H} of the high-temperature phase can be determined when the temperature is above T_2, and we suppose that C^{L} and C^{H} are constant under different pressures. Then, the entropy (S), which refers to the value at a given temperature T_0 for a heating run can be computed as[5]

$$S(T,p)=\begin{cases}\displaystyle\int_{T_0}^{T}\frac{C^{\mathrm{L}}}{T}\mathrm{d}T, & T<T_1,\\ \displaystyle S(T_1,p)+\int_{T_1}^{T}\frac{1}{T}\left(C+\frac{\mathrm{d}Q}{\mathrm{d}T}\right)\mathrm{d}T, & T_1<T\leqslant T_2,\\ \displaystyle S(T_2,p)+\int_{T_2}^{T}\frac{C^{\mathrm{H}}}{T}\mathrm{d}T, & T_2<T,\end{cases}\tag{1}$$

where

$$\frac{\mathrm{d}Q}{\mathrm{d}T}=\frac{\mathrm{d}Q/\mathrm{d}t}{\mathrm{d}T/\mathrm{d}t},$$

$\mathrm{d}Q/\mathrm{d}t$ is the heat flux measured by DSC, and $\mathrm{d}T/\mathrm{d}t$ is the heating rate. The specific heat C within the transition region equals $xC^{\mathrm{L}}+(1-x)C^{\mathrm{H}}$, where x is the percentage of the low-temperature phase. For a cooling run, an equivalent expression is similar except for the integration limits.

The entropy changes measured by quasi-direct methods (ΔS^{qd}) can be expressed as

$$\Delta S^{\mathrm{qd}}=S(T,p)-S(T,0),\tag{2}$$

where p is the applied pressure and $p=0$ indicates that the pressure is atmospheric pressure.

The temperature changes measured by quasi-direct methods (ΔT^{qd}) can be expressed as

$$\Delta T^{\mathrm{qd}}=T(S,p)-T(S,0).\tag{3}$$

The indirect methods are based on the Maxwell relations or Clausius–Clapeyron equation. For the BCE, the volume changes of the unit cell can be determined using x-ray diffraction under high pressure and different temperatures. However, as for the ECE, the stress(σ)–strain(ε) curves of elastocaloric materials can be obtained using suitable strain gauges. The equation of entropy changes can be expressed as follows:

Elastocaloric effects:

$$\Delta S[\mathrm{J\cdot K^{-1}\cdot m^{-3}}]=\int_{\sigma_{\mathrm{u}}^{\mathrm{i}}}^{\sigma_{\mathrm{u}}^{\mathrm{f}}}(\partial\varepsilon/\partial T)_{\sigma_{\mathrm{u}}'}\mathrm{d}\sigma_{\mathrm{u}}'.\tag{4}$$

Barocaloric effects:

$$\Delta S[\mathrm{J\cdot K^{-1}}]=-\int_{p^{\mathrm{i}}}^{p^{\mathrm{f}}}(\partial V/\partial T)_{p'}\mathrm{d}p',\tag{5}$$

where V is the volume of materials under pressure, 'i' and 'f' indicate the initial and final values, respectively.[3]

3. Mechanocaloric materials

Mechanocaloric materials can be classified into the following types of materials depending on their physical characteristics: non-magnetic shape memory alloys (non-MSMAs), magnetic shape memory alloys (MSMAs), magnetic materials, perovskite materials, oxyfluorides, polymers, superionic conductors, and plastic crystals.

3.1. Non-magnetic shape memory alloys

Shape memory alloys (SMAs) have many unique thermomechanical characteristics such as the shape memory effect, pseudoelasticity, and superelasticity. These alloys can 'memorize' their deformation and return to their original form when subjected to thermomechanical or magnetic variations. The non-MSMAs under uniaxial stress undergoes a reversible martensitic transition, which is a first-order structural transition. Because of the large latent heat of the transition, these alloys exhibit the MCE. The lattice distortion associated with the transition is mostly caused by a pure shear. The transition temperature and the MCE are strongly sensitive to uniaxial stress but insensitive to hydrostatic pressure.[8] Recently, research on the MCE of non-MSMAs has focused on Cu-based and Ti–Ni-based alloys. The thermal effect in single crystals of β-CuZnSn was reported in 1981.[9] Later experiments[10–13] have proved that Cu-based alloys such as Cu–Zn–Al single crystal have the MCE. ΔS and ΔT for Cu-based alloys can exceed 20 J·kg^{-1}·K^{-1} and 14 K, respectively. Because of the large value of ΔS and broad temperature span, the Cu–Zn–Al polycrystal has an enormous relative cooling power for the ECE.[11] Another important class of non-MSMAs is based on Ti–Ni.[7,14–22] These alloys transform from a B2 ($Pm2m$) to a B19′ ($P2/m$) martensitic phase upon cooling.[8] The reversible B2↔ B19′ transition has a large latent heat, and the transition entropy change is quite high (in the range of 60 J·kg^{-1}·K^{-1}–80 J·kg^{-1}·K^{-1}) at moderate stress ($\sim$ 170 MPa).[19] ΔT measured by direct methods can reach 25 K for Ni–Ti wires.[16,17] In addition, the cooling performance of Ni–Ti-based alloys has been studied. One study[7] revealed that Ni–Ti wires have a quite high cooling efficiency. Furthermore, the values of temperature changes for sputtered NiTi films, especially sputtered NiTiCu films, have good reproducibility even though the alloys have been trained for many cycles.[15,16] Recently, the ECE caused by the rubber-like behavior of the R-phase nanocrystalline wires of Ti–50.8Ni (at.%) has been reported. Because of the small energy dissipation, the ECE related to the R-phase is more efficient than that induced by the B2↔ B19′ transition.[23] The thermodynamic characteristics are compared for selected non-MSMAs in Table 1.

3.2. Magnetic shape memory alloys

Magnetic shape memory alloys (MSMAs) are interesting materials with mechano-caloric or multi-caloric effects. In MSMAs, the caloric effect is usually induced by a magnetostructural phase transition. Many characteristics of MSMAs are similar to those of non-MSMAs such as the martensitic transition and shape memory effects; however, the structural transition in MSMAs is accompanied by changes in the magnetism from the antiferromagnetic (AFM) state to the ferromagnetic (FM) state. MSMAs can be divided into two categories: Fe-based alloys, such as Fe–Pt and Fe–Pd, and Ni-based and some Co-based alloys, which are usually Heusler alloys. For MSMAs, the high-temperature phase is not martensitic but cubic and FM. As for the magnetism of the martensitic phase, it depends on whether the martensitic transition temperature is above or below the Curie temperature T_c in a specific material. The martensitic and magnetic transition in Fe-based MSMAs such as Fe–Pt and Fe–Pd were studied many years ago.[24–26] The martensitic transition from a cubic structure ($Fm3m$) to a face-centered tetragonal martensitic structure ($P4/mmm$) occurs on cooling for Fe-based MSMAs. In Fe–Pd alloys, the martensitic transition is weak first-order with a low entropy and small transformation hysteresis.[26] Because of the small volume changes of the unit cell in this transition, the BCE is not expected. The ECE was studied in Fe–Pd single crystal[26] and Fe_7Pd_3 polycrystal.[25] In Fe–31.2Pd (at.%) alloy, a significant ECE was reported. Because of lattice softening caused by a weak first-order martensitic transition near room temperature, an adiabatic temperature change of more than 3 K and ΔS of 4 J·kg^{-1}·K^{-1}–5 J·kg^{-1}·K^{-1} with excellent reproducibility were observed under uniaxial stress of 200 MPa in this alloy. Apart from Fe-based MSMAs, the MCE for Ni-based MSMAs belonging to Heusler alloys has been heavily investigated.[14,27–43] Early in their study, these investigated alloys were usually very brittle and could only support very low stresses ($\approx$ 10 MPa).[42,43] Later, tougher alloys were synthesized using suitable doping or other methods with the maximum applied stresses exceeding 300 MPa. The magnitude of the MCE in these MSMAs depends on the sensitivity of the martensitic transition to hydrostatic pressure or uniaxial stress. The MCE was observed in Ni-based magnetic shape memory alloys and can be compared with giant magnetocaloric effects. Upon uniaxial compression of 100 MPa, the stress-induced entropy change ΔS is 21 J·kg^{-1}·K^{-1} and the estimated ΔT is approximately 15 K in polycrystalline Ni–Mn–Sb–Co MSMA. The result is better than other reports on the ECE in Ni-based MSMAs.[24,29,39] For applied hydrostatic pressure, the BCE for Ni–Mn–In MSMA resulted from discontinuities of both the volume of the unit cell and entropy at a magnetostructural transition. This alloy exhibited both barocaloric and magnetocaloric effects. Under hydrostatic pressure of 260 MPa, ΔT can reach 4.5 K and ΔS is approximately 24 J·kg^{-1}·K^{-1}. However, when a magnetic field of 0.94 T is applied, the change of temperature for mCE is only 1.3 K.[27] It is worth noting that the peak values of ΔT and ΔS increase as pressure increases in the range of 20 MPa–260 MPa. These studies suggest that some magnetocaloric

materials could exhibit the BCE. Thermodynamic characteristics are compared for selected MSMAs in Tables 1 and 2.

3.3. Magnetic materials

Some magnetic materials also exhibit the MCE because of a first-order magnetostructural transition. The transition can cause changes in the symmetry of the crystal structure or just a uniform expansion or contraction of the unit cell. These compounds, which do not involve changes in the symmetry of the crystal structure, mainly include Fe–Rh, La–Fe–Si, and Mn–Ga–N compounds. The ECE in Fe–Rh alloys was reported early on.[44] The magnetic transformation from AFM to FM is accompanied by a negative temperature change of 5.2 K under stress of 529 MPa. Later, the BCE with good reproducibility in Fe–Rh alloys was observed.[45,46] Large values of $|\Delta T| \sim 8$ K–10 K and $|\Delta S| \sim 12$ J·kg^{-1}·K^{-1} were reported under hydrostatic pressure (250 MPa). Another class of these compounds is the La–Fe–Si-based itinerant ferromagnets. The $LaFe_{13-x}Si_x$ compounds have the cubic $NaZn_{13}$ structure ($Fm\bar{3}m$) and undergo a first-order magnetostructural transition related to BCE from a paramagnetic (PM) phase to FM phase. These contributions of the magnetism, lattice, and electrons to entropy changes in transition reduce the entropy for the FM low-temperature phase. Theoretical calculations indicate that ΔT and ΔS of the BCE can reach 16 K and 55 J·kg^{-1}·K^{-1}, respectively, under a pressure of 450 MPa in $La(Fe_{0.89}Si_{0.11})_{13}$.[47] Because of doping with Co to bring the transition temperature close to room temperature, many studies on the BCE in La–Fe–Si have focused on La–Fe–Co–Si compounds. The ΔS obtained using quasi-direct methods and ΔT measured by direct methods can reach 6 J·kg^{-1}·K^{-1} and 2 K, respectively, under a pressure of 200 MPa in $LaFe_{11.33}Co_{0.47}Si_{1.2}$.[48] Mn_3GaN is another itinerant antiferromagnetic system with an antiperovskite structure ($Pm\bar{3}m$). In this compound, a magnetic transition related to the BCE occurs from a PM phase to an AFM phase on cooling near 290 K. The magnetostructural transition enhanced by magnetic frustration leads to an isotropic expansion ($\sim 1\%$) of the unit cell.[49] ΔS obtained by quasi-direct methods and ΔT measured by direct and quasi-direct methods can reach 22 J·kg^{-1}·K^{-1}, 1.5 K, and 4.5 K, respectively, under a pressure of 150 MPa in Mn_3GaN. Unlike the above magnetic materials, there are some materials whose BCE is accompanied by changes in the crystal structure symmetry. For example, the BCE in $Gd_5Si_2Ge_2$ compounds was studied under pressure.[50–52] These compounds undergo a phase transition from a monoclinic ($P112_1/a$) PM phase toward an orthorhombic (*Pnma*) FM phase upon cooling.[53] At 200 MPa, the maximum of the entropy changes of 11 J·kg^{-1}·K^{-1} and ΔT^{d} of approximately 1 K are less than those estimated from entropy data. The last mainly magnetic material family with the BCE is the Mn-based ternary compounds whose formula can be expressed as MnTX (T = Ni, Co and X = Si, Ge). These compounds undergo a second-order magnetic phase transition from a PM phase toward another magnetic phase relying on the particular composition. When the temperature drops, there is a structural transition from a Ni_2In-type hexagonal phase ($P6_3/mmc$) to a TiNiSi-type orthorhombic structure (*Pnma*) in MnTX. Through doping, varying the composition, and isostructural substitution, the alloys only exhibit a magnetostructural transition. The BCE was reported in $MnCoGe_{0.99}In_{0.01}$ compound.[54] The BCE induced by magneto-structure transition has a large ΔS (50 J·kg^{-1}·K^{-1}–74 J·kg^{-1}·K^{-1}) and ΔT (16 K–19 K), which were measured using quasi-direct methods at pressures of 300 MPa. ΔT is higher than that measured by direct methods (3 K–8 K) and lower than that estimated from the entropy change (33 K–36 K). The transition temperature, *i.e.*, the work temperature of magnetic materials, can be adjusted by doping or using other methods. The feature is useful under some special conditions. The thermodynamic characteristics are compared for selected materials in Tables 1 and 2.

3.4. Perovskite materials

Perovskite materials have the same crystal structure as calcium titanium oxide, known as the perovskite structure. The general chemical formula for perovskite materials is ABX_3, where A and B are two cations of very different sizes and X is an anion that bonds to both A and B.[55] For cubic structure stability, the requirement of relative ion size is very stringent. Therefore, slight distortion and deformation can result in several lower-symmetry structures, in which the coordination number of A or B cations or both is reduced. These characteristics lead to a rich phase diagram in perovskite materials. Furthermore, many perovskite ceramics such as $BaTiO_3$ exhibit ferroelectricity because the complex structure produces electric dipoles. The perovskite materials mentioned in this section are also ferroelectric materials, which were investigated as eCE materials. Because of the strong coupling between polarization and structure, ferroic phase transitions may occur in perovskite materials. Therefore, the MCE is expected in perovskite materials. The MCE of perovskite materials such as $BaTiO_3$, $(Ba_{0.85}Ca_{0.15})(Zr_{0.1}Ti_{0.9})O_3$, and $PbTiO_3$ has been investigated.[56–64] At high temperature (> 400 K), $BaTiO_3$ has a centrosymmetric ABO_3 perovskite crystal structure ($Pm\bar{3}m$). When the temperature decreases from above 400 K to below 180 K, this material will exhibit two ferroelectric–structural and three structural phase transitions. At the first ferroelectric phase transition temperature

($\sim$ 400 K), the cubic structure transforms to a tetragonal structure ($P4mm$) with volume expansion ($\sim$ 0.11%) of the unit cell. The second phase transition occurs at approximately 270 K, and the tetragonal phase transforms toward a ferroelectric orthorhombic phase ($Bmm2$). The last structure transition is the orthorhombic–rhombohedral transition near 180 K. An entropy change with the BCE has been reported. ΔS for the cubic-tetragonal and tetragonal–orthorhombic transition is 1.7 J·kg^{-1}·K^{-1} and 1.2 J·kg^{-1}·K^{-1}, respectively, and the values were determined using DSC under hydrostatic pressure of 100 MPa. The MCE was also reported in ferroelectric $PbTiO_3$. Molecular dynamic simulation predicted the ECE in $PbTiO_3$ with ΔT of 25 K and 44 K under stresses of 0.5 GPa and 2 GPa, respectively.[58] The compound is a cubic perovskite structure at much higher temperature ($\sim$ 700 K). On cooling, it exhibits a first-order structural phase transition. This transition between a cubic and tetragonal phase ($P4mm$) accompanies a paraelectric–ferroelectric transition. The absolute values of ΔT and ΔS for the BCE are 1.9 K and 2.7 J·kg^{-1}·K^{-1}, respectively, under the hydrostatic pressure of 260 MPa.[63] According to a recent report, the peak values of ΔT for the ECE in lead zirconate titanate are 0.2 K and 1.25 K under stresses of 100 MPa and 400 MPa, respectively, near room temperature (300 K).[60] In perovskites, the BCE is more significant when the pressure is increased. For example, the maximum ΔT for the BCE in $BaTiO_3$ single crystals is 2.8 K and 3.6 K when the applied pressure is 0.6 GPa and 2.4 GPa, respectively.[57] These perovskites exhibit excellent hardness and stability. However, their cooling efficiency is inadequate under low pressure.

As special perovskites, organic–inorganic hybrid perovskites exhibit pressure-induced solid-state cooling effects. This family of materials has the perovskite structure ABX_3, where A is an alkylammonium cation, B is a transition metal cation, and X is a halide or polyatomic bidentate-bridge ligand. A prior review summarized the BCE in more than a dozen hybrid perovskites.[65] These hybrid perovskites have the following characteristics: (i) a large and reversible entropy change, (ii) a large shift of transition temperature with pressure, and (iii) an adequate transition temperature. A typical example of hybrid perovskites is [TPrA]Mn[dca]$_3$ (TPrA = $(CH_3CH_2CH_2)_4N^+$, dca = $[N(CN)_2]^-$).[66] This material exhibits giant BCEs near room temperature under a pressure of 70 bar (1 bar = 10^5 Pa).

3.5. Polymers

Unlike the above MCE materials, the MCE materials discussed in this section are amorphous. This type of material can support a dramatic reversible elongation or retraction. The huge deformation results in a huge entropy change. In fact, the first reported material with the ECE is Indian rubber, a randomly oriented polymer.[1] However, this material was not valued until recently.[67–70] In natural rubber, the highest temperature change for the ECE is 13.7 K at 674% elongation and the estimated ΔS is 67 J·kg^{-1} K^{-1}. There are many polymers with the MCE based on ferroelectric polymers such as polyvinylidene fluoride (PVDF).[71–74] According to results of x-ray diffraction experiments, a crystal transformation from the anti-polar α to the polar β phase was observed in PVDF terpolymers. The transformation can be induced by pressure or an electric field. The elastocaloric properties of PVDF trifluoroethylene chlorotrifluoroethylene (PVDF–TrEE–CTFE) were reported using an infrared imaging camera. ΔT of 2.15 K and ΔS of 11 J·kg^{-1}·K^{-1} were measured at a strain of 12%. For the BCE, ΔT of 6 K in this polymer was observed under a pressure of 200 MPa at room temperature and increased to approximately 19 K at the phase transition temperature of 368 K.

3.6. Rare-earth compounds

The MCE of rare-earth compounds as solid-state cooling materials was studied. Because of their 4f electron hybrids, most rare-earth materials have rich magnetic properties that are sensitive to pressure. Some rare-earth compounds such as $Ce_x(La, Y)_{1-x}Sb$, HoAs, $Ce_3Pd_{20}Ge_6$, and $EuNi_2(Si_{1-x}Ge_x)_2$ have been reported as MCE materials.[75–78] In these compounds, the entropy changes must take into account that the crystalline electric field splits the $(2J+1)$-fold degenerated ground-state J-multiplet of the rare-earth ion into discrete energy levels. In $Ce_x(La, Y)_{1-x}Sb$, the PM–AFM transition induced by uniaxial stress was expected to result in a huge entropy change. The *in situ* experiments revealed ΔT of 0.42 K upon releasing a uniaxial stress of 240 MPa in $Ce_{0.85}(La_{0.95}Y_{0.05})_{0.15}Sb$ and ΔT of 2 K upon releasing a uniaxial stress of 500 MPa in CeSb at low temperature ($\sim$ 20 K). The monopnictide HoAs exhibits the ECE resulting from a magnetic–structural phase transition. ΔT for the ECE is over 0.4 K upon the application of uniaxial stress of 300 MPa along the [001] direction. The third material introduced is a heavy-fermion system $Ce_3Pd_{20}Ge_6$. The $|\Delta T|$ of 0.75 K for the ECE was obtained in the Kondo lattice compound $Ce_3Pd_{20}Ge_6$ because release of the uniaxial stress of 300 MPa leads to a positive shift of the Kondo temperature and splitting of the ground state at 4.4 K. The rare-earth compound $EuNi_2(Si_{1-x}Ge_x)_2$ undergoes a first-order valence transition with a thermal hysteresis of 10 K and a huge entropy change from an Eu^{2+} state toward an Eu^{3+} state near 42 K. The sharp valence transition is expected to lead to the BCE.

3.7. Oxyfluorides

In the year 2010, the MCE in a series of oxyfluorides was reported. These oxyfluorides have four types, namely $(NH_4)_2NbOF_5$, $(NH_4)_2WOF_4$, $(NH_4)_2MoO_2F_4$, and Rb_2KTiOF_5.[79–83] The ammonia compound $(NH_4)_2NbOF_5$ undergoes two phase transitions accompanied by entropy changes. For $(NH_4)_2NbOF_5$, the disordered phase I transforms into the partially ordered phase II on cooling at 258 K and then transforms to a fully ordered phase III at 220 K.[84] The strengths of the BCE and ECE are almost equal. The maximum of ΔT and ΔS for the MCE can reach 15 K and 60 J·kg^{-1}·K^{-1}, respectively, upon the application of hydrostatic pressure or uniaxial stress of 1 GPa near the phase transition temperatures. Later, the MCE in $(NH_4)_2WOF_4$ and $(NH_4)_2MoO_2F_4$ oxyfluorides was studied. Two phase transitions were reported at 271.4 K and 180 K for the molybdate and at 201.5 K and 161 K for the tungstate. ΔT of 10 K and ΔS of 40 J·kg^{-1}·K^{-1} for the molybdate and ΔT of 12 K and ΔS of 50 J·kg^{-1}·K^{-1} for the tungstate were calculated using differential thermal analysis under a force field of 0.5 GPa near the first-order structural phase transitions. Later, the MCE in Rb_2KTiOF_5 was observed near the structural phase transition at 215 K under pressure between 0 and 0.6 GPa. The Rb_2KTiOF_5 undergoes a first-order ferroelastic phase transition that can result in huge entropy changes. ΔT of 16 K and ΔS of 43 J·kg^{-1}·K^{-1} were calculated from the differential thermal analysis under a pressure of 0.4 GPa. In 2016, a review of the MCE in ferroelastic fluorides and oxyfluorides was published.[83] This paper reviewed the effects of uniaxial stress and hydrostatic pressure on phase transitions, the MCE, and the experiment methods used to obtain the temperature–pressure phase diagram and entropy under high pressure. The thermodynamic characteristics of selected materials are compared in Table 2. Oxyfluorides have a good cooling efficiency under moderate pressure but are not very stable in air.

3.8. Superionic conductors

Superionic conductors, also known as fast ionic conductors, are a class of solid materials with extremely high ionic conductivity.[85] According to recent studies of the BCE in fluoride-based and AgI superionic conductors, superionic conductors are expected to be good candidates for MCE materials.[86,87] The superionic transition in fluorite-structured fast ion conductors such as CaF_2 and PbF_2 results in a large entropy change of over 100 J·kg^{-1}·K^{-1} under hydrostatic pressure or uniaxial stress. $|\Delta T|$ of 20 K in PbF_2 and 3 K in CaF_2 were calculated using density functional theory upon releasing the stress of 0.6 GPa. When the hydrostatic pressure increases to 5 GPa, calculations for the BCE in CaF_2 indicate that $|\Delta T|$ and $|\Delta S|$ can reach 152 K and 186 J·kg^{-1}·K^{-1}, respectively. Other materials with giant MECs include AgI, which consists of α, β, and γ phases at different temperatures. The structure of the α phase is a body-centered-cubic structure ($Im\bar{3}m$). The structures of the β and γ phases are a hexagonal-close-packed structure ($P\bar{6}_3mc$) and a cubic-close-packed structure ($F\bar{4}3m$), respectively. The first-order structural phase transition from the superionic α phase to a mixed phase of β and γ leads to a disorder–order transition of the silver cations on cooling at approximately 420 K. Because of the first-order reconstructive phase transition with a huge volume change (5%) of the unit cell, the entropy change in the transition can reach 63 ± 4 J·kg^{-1}·K^{-1}. The solid electrolyte AgI exhibits the BCE. ΔT of 18 K and ΔS of 60 J·kg^{-1}·K^{-1} were observed near the superionic phase transitions. However, AgI and similar superionic conductor such as AgBr and AgCl are unstable owing to photolysis.

3.9. Plastic crystals (orientation-disordered crystals)

In 2019, colossal BCEs were observed in plastic crystals.[88,89] Plastic crystals, also known as orientation-disordered crystals, are oriented randomly, whereas the mass center forms symmetric lattices. The reversible first-order transition induced by pressure in plastic crystals induces large amounts of heat changes. In plastic crystals such as 2,2-dimethyl-1,3-propanediol (NPG), 2-methyl-2-nitro-1-propanol (MNP), and pentaglycerin (PG), the solid-state transition enthalpy is equivalent to or even higher than the melting enthalpy of some common solids such as Fe, Ti, and Mn. For the BCE in NPG, MNP, and PG, the maximum of $|\Delta S|$ calculated by indirect methods can reach 389, 404, and 493 J·kg^{-1}·K^{-1}, respectively. The value of entropy changes in plastic materials is dozens of times as large as that in previous materials with the MCE. The microscopic origin of colossal BCEs in plastic crystals was revealed through high-resolution quasi-elastic neutron scattering and inelastic neutron scattering experiments under high pressure. These experiments verified that orientational disorder in plastic crystals is restrained by the pressure. Thus, the transition results in huge entropy changes.[88] Plastic crystals have excellent cooling efficiency; however, the organic part leads to quite large hysteresis.

To date, the MCE has been investigated in SMAs including non-magnetic SMAs and MSMAs, ferroelectric perovskite materials, polymers, rare-earth compounds, oxyfluorides, superionic conductors, plastic crystals, and other materials. Here, we list thermodynamic characteristics for the elastocaloric effect (in Table 1) and barocaloric effect (in Table 2) in selected materials.

Table 1. Thermodynamic characteristics for elastocaloric effect compounds. Temperature for the forward (cooling) transition (T_t); transition temperature shift with uniaxial stress ($dT/d\sigma$); applied stress ($\Delta\sigma$) to obtain the temperature and entropy changes in this table; adiabatic temperature change measured using direct methods (ΔT^d) and estimated from the measured isothermal entropy change (ΔT^e); isothermal entropy change determined using indirect methods (ΔS^i) and estimated from measured temperature changes (ΔS^e).

Compound	Sample status	T_t/K	$(dT/d\sigma)$/(K/GPa)	$\lvert\Delta T^d\rvert$/K	$\lvert\Delta T^e\rvert$/K	$\lvert\Delta S^i\rvert$ /J·kg^{-1}·K^{-1}	$\lvert\Delta S^e\rvert$ /J·kg^{-1}·K^{-1}	$\Delta\sigma$/GPa	Reference
$Cu_{68.13}Zn_{15.74}Al_{16.13}$	single crystal	234	500	6	11	20.7	11	0.12	[10,13]
$Cu_{68}Zn_{16}Al_{16}$	ploy crystal	205	513	6	12	17.9	13	0.25	[11]
$Cu_{83}Al_{14}Ni_3$	single crystal	250	500 ± 50	14	–	–	26	0.15	[93]
$Ni_{50.38}Ti_{49.62}$	single crystal	220	120	14	–	–	51	0.5	[14]
NiTi	wire	300	–	25.5	–	–	46	0.55	[16]
$Ni_{48.9}Ti_{51.1}$	wire	295	132	25	–	–	46	0.8	[17]
$Ni_{47.9}Ti_{52.6}$	wire	320	200	–	38	60–80	–	0.18	[19]
$Ni_{47.9}Ti_{52.6}$	wire	310	50	–	8	12	—	0.18	[19]
$Ni_{50}Ti_{50}$	film	260	–	16	–	–	26	0.3	[94]
$Fe_{49}Rh_{51}$	poly crystal	315	−20	5.2	–	–	7	0.53	[44]
$Fe_{68.8}Pd_{31.2}$	single crystal	230	−1000	3	–	–	5	0.2	[26]
$Ni_{50}Fe_{19}Ga_{27}Co_4$	single crystal	300	400	10	–	–	15	0.3	[95]
$Co_{40}Ni_{33.17}Al_{26.83}$	single crystal	303	400	3	–	–	5	0.05	[14]
$Ni_{43}Mn_{40}Sn_{10}Cu_7$	poly crystal	322	200	–	1.5	2	–	0.01	[28]
$Ni_{46}Mn_{38}Sb_{12}Co_4$	poly crystal	300	130	–	15	20	–	0.1	[30]
$Ni_{43.5}Mn_{39}Sn_{11}Co_{6.5}$	poly crystal	260	100	–	6	12	–	0.3	[37]
$Ni_{45}Mn_{44}Sn_{11}$	poly crystal	270	–	6	–	–	13	0.26	[36]
$Ni_{45}Mn_{36.4}In_{13.6}Co_5$	poly crystal	250	240	4	–	–	5	0.15	[33]
$(Ni_{50}Mn_{31.5}Ti_{18.5})_{99.8}B_{0.2}$	poly crystal	308		31.5	–	45	–	0.7	[92]

Table 2. Thermodynamic characteristics for the barocaloric effect compounds.

Compound	Sample status	T_t/K	(dT/dp)/(K/GPa)	$\lvert\Delta T^d\rvert$/K	$\lvert\Delta T^{qd}\rvert$/K	$\lvert\Delta T^e\rvert$/K	$\lvert\Delta S^{qd}\rvert$ /J·kg^{-1}·K^{-1}	Δp/GPa	Reference
$Fe_{49}Rh_{51}$	poly crystal	310	64	–	9	8	12	0.25	[45]
$LaFe_{11.33}Co_{0.47}Si_{1.2}$	Poly crystal	250	−94	2.2	–	5	8.6	0.2	[48]
Mn_3GaN	–	290	−65	1.3	4.5	14	22.3	0.14	[49]
$Gd_5Si_2Ge_2$	poly crystal	260	35	1	–	10	11	0.2	[50,51]
$MnCoGe_{0.99}In_{0.01}$	poly crystal	310	−77	8.4	18.5	36	52	0.3	[96]
$(MnNiSi)_{0.62}$ $(FeCoGe)_{0.38}$	Poly crystal	338	-75	3	16	33	74	0.27	[97]
$Ni_{49.26}Mn_{36.08}In_{14.66}$	poly crystal	290	18	–	4.5	18	24	0.26	[27]
$Ni_{50}Mn_{33}In_{17}$	poly crystal	275	19	–	3	9	13	0.25	[34]
$Ni_{51}Mn_{33}In_{16}$	poly crystal	330	18	–	4	29	35	0.25	[34]
$Ni_{42.7}Co_{8.87}Mn_{31.67}$ $Ga_{14.98}In_{2.01}$	–	400	30	–	–	16	16	0.25	[98]
$BaTiO_3$	single crystal	400	−55	–	1	2	1.6	0.1	[61]
$BaTiO_3$	single crystal	280	−30	–	–	1	1.3	0.1	[61]
$PbTiO_3$	single crystal	770	−140	2.7	–	1.9	4	0.26	[63]
$(NH_4)_2SO_4$	single crystal	220	-50 ± 10	–	–	8	60	0.15	[90]
[TPrA]Mn[dac]$_3$	poly crystal	330	231	–	5	–	37	0.007	[66]
$(NH_4)_2NbOF_5$	single crystal	259.3,220.5	−45	–	15	25	100	1	[79]
$(NH_4)_2MoOF_4$	single crystal	271.4	92.8	–	17	17	73	0.9	[80]
$(NH_4)_2WOF_4$	single crystal	201.5	13	–	13	9	40	0.5	[80]
$(NH_4)_2SnF_6$	single crystal	110 ± 1	−157	–	11	11	61	0.14	[99]
Rb_2KTiOF_5	–	215	110	–	18	15	46	0.6	[82]
AgI	polymorph	420	−128±5	–	18	–	60	0.25	[87]
NPG	–	320	93 ± 18	–	~45	–	~510	0.6	[89]

Figure 1 shows ΔT and ΔS for selected mechanocaloric materials under hydrostatic pressure or uniaxial stress. These current studies have shown that the application external hydrostatic pressure or uniaxial stress is a very effective and clean method to induce structural transitions and change the entropy and temperature of the crystals or amorphous polymers. In ferromagnetic or ferroelectric materials, the pressure affects the structure, magnetization, or polarization. Generally, the transition temperature shifts under different pressure. The shift coefficient dT/dp or $dT/d\sigma$ represents the sensi-

tivity of the transition to hydrostatic pressure or uniaxial stress. Many materials with the MCE have been discovered near ferroic phase transitions.[3] Therefore, we expect the MCE could be observed in magnetocaloric and/or electrocaloric materials. In addition to mechanocaloric materials associated with pure structural, magnetostructural, or electrostructural transitions, polymers and plastic crystals exhibit colossal MCEs associated with disorder–order transitions. The application of pressure suppresses the oriented disorder in polymers and plastic crystals. However, the obvious drawback is a large hysteresis of the disorder–order transition in polymers.[91] After dozens of minutes, the materials can carry out the next cycle. In addition, the organic matter and superionic conductors are not stable enough in air. According to current research on their mechanical performance, hysteresis, and cooling efficiency, SMAs are good candidates for widespread applications. These alloys have been intensively investigated for a long time. A very recent study reported colossal MCEs with a strikingly high value of 31.5 K in a Ni–Mn-based Heusler SMA.[92] In fact, the disorder–order transition has a larger value of entropy change than structural transition in this SMA. The potential materials with the disorder–order transition are expected to have a feature that part of the ions or ionic groups can freely move but the remaining ions or ionic groups are stable and maintain structural symmetry. Therefore, these materials should have the advantages of both SMAs and polymers. In this case, the materials will have a small hysteresis and large entropy changes similar to organic–inorganic hybrid materials and superionic conductors.

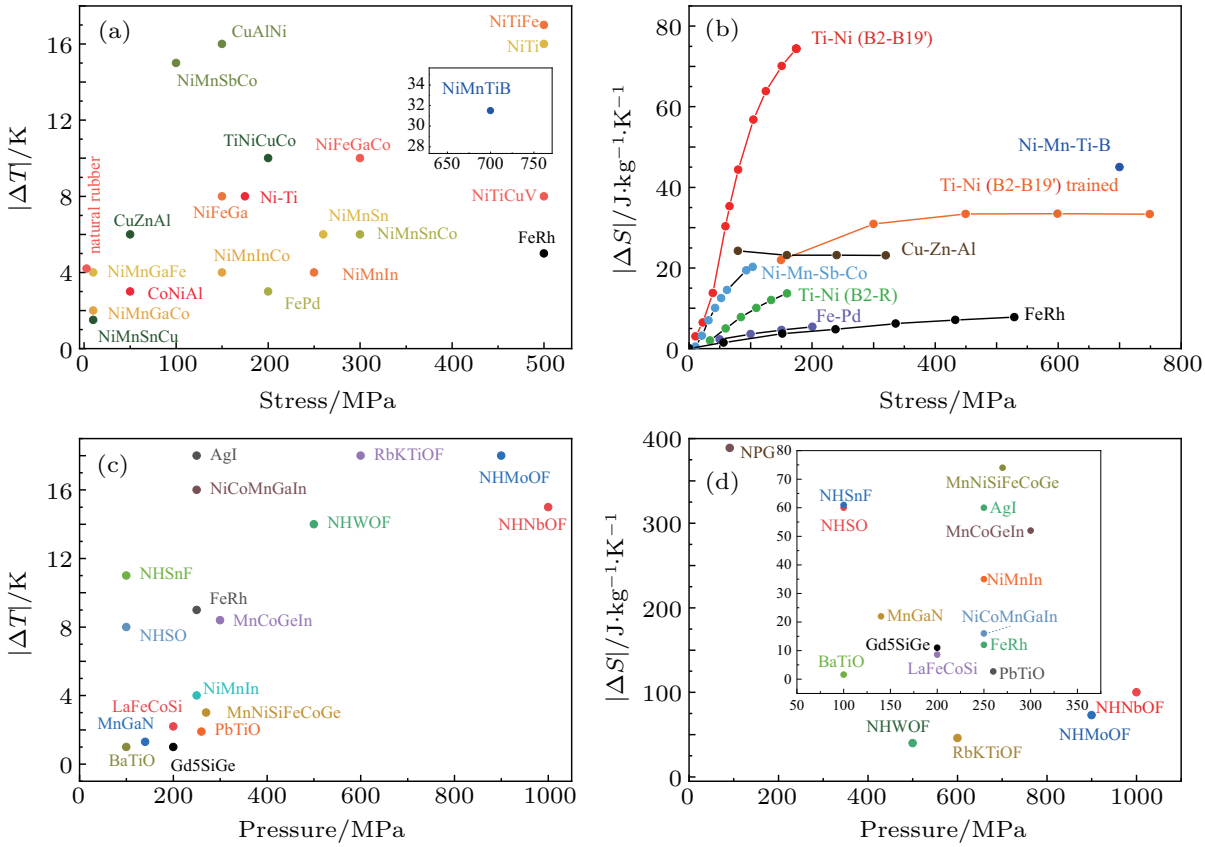


Fig. 1. (a) and (b) Absolute value for the isothermal entropy change and adiabatic temperature change, respectively, as a function of the applied uniaxial stress for selected elastocaloric materials. (c) and (d) Absolute value of isothermal entropy change and adiabatic temperature change, respectively, as a function of the hydrostatic pressure for selected barocaloric materials.

4. Conclusion

In conclusion, to boost the application of mechanocaloric materials, we reviewed the measurement techniques for the mechanocaloric effect and reviewed mechanocaloric materials. From an application viewpoint, we propose requirements that a good refrigerant should meet. Through analysis of the mechanocaloric effect in various mechanocaloric materials, we summarize and compare the characteristics of these materials. Finally, we suggest that a material with the disorder–order transition and small hysteresis can exhibit a more significant caloric effect and is more suitable for application in solid-state cooling.

Acknowledgment

We are indebted to all PhD students and senior colleagues with whom we have been collaborating for many years on the topics covered in this paper.

References

[1] Gough J 1805 *Manchester Phil. Mem.* Second Series **1** 288
[2] Joule J P 1859 *Philos. Trans. R. Soc. London* **149** 91
[3] Moya X, Kar-Narayan S and Mathur N D 2014 *Nat. Mater.* **13** 439
[4] Lu B and Liu J 2015 *Sci. Bull.* **60** 1638
[5] Manosa L and Planes A 2017 *Adv. Mater.* **29** 1603607
[6] Tusek J, Engelbrecht K, Millan-Solsona R, Manosa L, Vives E, Mikkelsen L P and Pryds N 2015 *Adv. Energy Mater.* **5** 1500361
[7] Ossmer H, Miyazaki S and Kohl M 2015 *Mater. Today-Proc.* **2** 971
[8] Manosa L and Planes A 2016 *Philos. Trans. R. Soc. A* **374** 20150310
[9] Brown L C 1981 *Metall. Mater. Tran. A* **12** 1491
[10] Bonnot E, Romero R, Manosa L, Vives E and Planes A 2008 *Phys. Rev. Lett.* **100** 125901
[11] Mañosa L, Jarque-Farnos S, Vives E and Planes A 2013 *Appl. Phys. Lett.* **103** 211904
[12] Qian S, Geng Y L, Wang Y, Pillsbury T E, Hada Y, Yamaguchi Y, Fujimoto K, Hwang Y H, Radermacher R, Cui J, Yuki Y J, Toyotake K and Takeuchi I 2016 *Philos. Trans. R. Soc. A* **374** 20150309
[13] Vives E, Burrows S, Edwards R S, Dixon S, Mañosa L, Planes A and Romero R 2011 *Appl. Phys. Lett.* **98** 011902
[14] Pataky G J, Ertekin E and Sehitoglu H 2015 *Acta Mater.* **96** 420
[15] Bechtold C, Chluba C, Lima de Miranda R and Quandt E 2012 *Appl. Phys. Lett.* **101** 091903
[16] Cui J, Wu Y, Muehlbauer J, Hwang Y, Radermacher R, Fackler S, Wuttig M and Takeuchi I 2012 *Appl. Phys. Lett.* **101** 073904
[17] Tušek J, Engelbrecht K, Mikkelsen L P and Pryds N 2015 *J. Appl. Phys.* **117** 124901
[18] Schmidt M, Frenzel J, Seelecke S, Ullrich J, Schutze A, Wieczorek A and Eggeler G 2016 *Asme Conference on Smart Materials, Adaptive Structures and Intelligent Systems*, September 21–23 2015 Colorado Springs, Colorado, USA, p. 9
[19] Soto-Parra D, Vives E, Manosa L, Matutes-Aquino J A, Flores-Zuniga H and Planes A 2016 *Appl. Phys. Lett.* **108** 071902
[20] Tusek J, Engelbrecht K and Pryds N 2016 *Sci. Technol. Built. En.* **22** 489
[21] Xiao F, Fukuda T and Kakeshita T 2016 *Scr. Mater.* **124** 133
[22] Luo X H, Ren W J, Jin W and Zhang Z D 2017 *Chin. Phys. B* **26** 036501
[23] Liang X, Xiao F, Jin M J, Jin X J, Fukuda T and Kakeshita T 2017 *Scr. Mater.* **134** 42
[24] Kakeshita T and Ullakko K 2002 *MRS Bull.* **27** 105
[25] Cui J, Shield T W and James R D 2004 *Acta Mater.* **52** 35
[26] Xiao F, Fukuda T, Kakeshita T and Jin X 2015 *Acta Mater.* **87** 8
[27] Manosa L, Gonzalez-Alonso D, Planes A, Bonnot E, Barrio M, Tamarit J L, Aksoy S and Acet M 2010 *Nat. Mater.* **9** 478
[28] Castillo-Villa P O, Manosa L, Planes A, Soto-Parra D E, Sanchez-Llamazares J L, Flores-Zuniga H and Frontera C 2013 *J. Appl. Phys.* **113** 053506
[29] Lu B F, Xiao F, Yan A and Liu J 2014 *Appl. Phys. Lett.* **105** 161905
[30] Millan-Solsona R, Stern-Taulats E, Vives E, Planes A, Sharma J, Nayak A K, Suresh K G and Manosa L 2014 *Appl. Phys. Lett.* **105** 241901
[31] Huang C, Wang Y, Tang Z, Liao X, Yang S and Song X 2015 *J. Alloys Compd.* **630** 244
[32] Huang Y J, Hu Q D, Bruno N M, Chen J H, Karaman I, Ross J H and Li J G 2015 *Scr. Mater.* **105** 42
[33] Lu B, Zhang P, Xu Y, Sun W and Liu J 2015 *Mater. Lett.* **148** 110
[34] Stern-Taulats E, Planes A, Lloveras P, Barrio M, Tamarit J L, Pramanick S, Majumdar S, Yüce S, Emre B, Frontera C and Mañosa L 2015 *Acta Mater.* **96** 324
[35] Li Y, Zhao D W and Liu J 2016 *Sci. Rep.* **6** 25500
[36] Sun W, Liu J, Lu B F, Li Y and Yan A 2016 *Scr. Mater.* **114** 1
[37] Yang Z, Cong D Y, Huang L, Nie Z H, Sun X M, Zhang Q H and Wang Y D 2016 *Mater.* **92** 932
[38] Camarillo J P, Aguilar-Ortiz C O, Flores-Zuniga H, Rios-Jara D, Soto-Parra D E, Stern-Taulats E, Manosa L and Planes A 2017 *Funct. Mater. Lett.* **10** 1740007
[39] Shen Q, Zhao D W, Sun W, Li Y and Liu J 2017 *J. Alloys Compd.* **696** 538
[40] Yang Z, Cong D Y, Sun X M, Nie Z H and Wang Y D 2017 *Acta Mater.* **127** 33
[41] Zhao D W, Liu J, Feng Y, Sun W and Yan A 2017 *Appl. Phys. Lett.* **110** 021906
[42] Soto-Parra D E, Vives E, González-Alonso D, Mañosa L, Planes A, Romero R, Matutes-Aquino J A, Ochoa-Gamboa R A and FloresZ úñiga H 2010 *Appl. Phys. Lett.* **96** 071912
[43] Castillo-Villa P O, Soto-Parra D E, Matutes-Aquino J A, Ochoa-Gamboa R A, Planes A, Mañosa L, González-Alonso D, Stipcich M, Romero R, Ríos-Jara D and Flores-Zúñiga H 2011 *Phys. Rev. B* **83** 174109
[44] Nikitin S A, Myalikgulyev G, Annaorazov M P, Tyurin A L, Myndyev R W and Akopyan S A 1992 *Phys. Lett. A* **171** 234
[45] Stern-Taulats E, Planes A, Lloveras P, Barrio M, Tamarit J L, Pramanick S, Majumdar S, Frontera C and Mañosa L 2014 *Phys. Rev. B* **89** 214105
[46] Stern-Taulats E, Gràcia-Condal A, Planes A, Lloveras P, Barrio M, Tamarit J L, Pramanick S, Majumdar S and Mañosa L 2015 *Appl. Phys. Lett.* **107** 152409
[47] de Medeiros L G, de Oliveira N A and Troper A 2008 *J. Appl. Phys.* **103** 113909
[48] Manosa L, Gonzalez-Alonso D, Planes A, Barrio M, Tamarit J L, Titov I S, Acet M, Bhattacharyya A and Majumdar S 2011 *Nat. Commun.* **2** 595
[49] Matsunami D, Fujita A, Takenaka K and Kano M 2015 *Nat. Mater.* **14** 73
[50] Yuce S, Barrio M, Emre B, Stern-Taulats E, Planes A, Tamarit J L, Mudryk Y, Gschneidner K A, Pecharsky V K and Mañosa L 2012 *Appl. Phys. Lett.* **101** 071906
[51] Zou J D 2012 *Chin. Phys. B* **21** 037503
[52] de Oliveira N A 2013 *J. Appl. Phys.* **113** 033910
[53] Pecharsky V K and Gschneidner Jr K A 2001 *Adv. Mater.* **13** 683
[54] Wu R R, Bao L F, Hu F X, Wu H, Huang Q Z, Wang J, Dong X L, Li G N, Sun J R, Shen F R, Zhao T Y, Zheng X Q, Wang L C, Liu Y, Zuo W L, Zhao Y Y, Zhang M, Wang X C, Jin C Q, Rao G H, Han X F and Shen B G 2016 *Sci. Rep.* **6** 22826
[55] Navrotsky A 1998 *Chem. Mater.* **10** 2787
[56] Liu Y, Wei J, Janolin P E, Infante I C, Kreisel J, Lou X J and Dkhil B 2014 *Phys. Rev. B* **90** 104107
[57] Liu Y, Wei J, Janolin P E, Infante I C, Lou X and Dkhil B 2014 *Appl. Phys. Lett.* **104** 162904
[58] Barr J A, Beckman S P and Nishimatsu T 2015 *J. Phys. Soc. Jpn.* **84** 024716
[59] Chauhan A, Patel S and Vaish R 2015 *Appl. Phys. Lett.* **106** 172901
[60] Patel S, Chauhan A and Vaish R 2016 *Energy Tehnol.* **4** 647
[61] Stern-Taulats E, Lloveras P, Barrio M, Defay E, Egilmez M, Planes A, Tamarit J L, Manosa L, Mathur N D and Moya X 2016 *APL Mater.* **4** 091102
[62] Wang F, Li B, Ou Y, Liu L F, Peng C Z, Wang Z S and Wang W 2016 *RSC Adv.* **6** 70557
[63] Mikhaleva E A, Flerov I N, Gorev M V, Molokeev M S, Cherepakhin A V, Kartashev A V, Mikhashenok N V and Sablina K A 2012 *Phys. Solid State* **54** 1832
[64] Lisenkov S and Ponomareva I 2012 *Phys. Rev. B* **86** 104103
[65] Bermudez-Garcia J M, Sanchez-Andujar M and Senaris-Rodriguez M A 2017 *J. Phys. Chem. Lett.* **8** 4419
[66] Bermudez-Garcia J M, Sanchez-Andujar M, Castro-Garcia S, Lopez-Beceiro J, Artiaga R and Senaris-Rodriguez M A 2017 *Nat. Commun.* **8** 15715
[67] Dart S L, Anthony R L and Guth E 1942 *Ind. Eng. Chem.* **34** 1340
[68] Xie Z, Sebald G and Guyomar D 2016 *Appl. Phys. Lett.* **108** 041901
[69] Xie Z J, Sebald G and Guyomar D 2017 *Appl. Therm. Eng.* **111** 914
[70] Sakata A, Suzuki N, Higashiura Y, Matsuo T and Sato T 2013 *J. Therm. Anal. Calorim.* **113** 1555
[71] Rodriquez E L and Filisko F E 1982 *J. Appl. Phys.* **53** 6536
[72] Roland C M, Garrett J T, Casalini R, Roland D F, Santangelo P G and Qadri S B 2004 *Chem. Mater.* **16** 857
[73] Patel S, Chauhan A, Vaish R and Thomas P 2016 *Appl. Phys. Lett.* **108** 072903
[74] Yoshida Y, Yuse K, Guyomar D, Capsal J F and Sebald G 2016 *Appl. Phys. Lett.* **108** 242904
[75] Strässle T and Furrer A 2000 *High Press. Res.* **17** 325

[76] Strasslea T, Furrer A, Altorfer F, Mattenberger K, Böhm M and Mutka H 2001 *J. Alloys Compd.* **323–324** 392
[77] Strässle T, Furrer A, Dönni A and Komatsubara T 2002 *J. Appl. Phys.* **91** 8543
[78] Hossain Z, Strässle T, Geibel C and Furrer A 2004 *J. Magn. Magn. Mater.* **272-276** 2352
[79] Gorev M, Bogdanov E, Flerov I and Laptash N 2010 *J. Phys.: Condens. Matter* **22** 185901
[80] Gorev M V, Bogdanov E V, Flerov I N, Kocharova A G and Laptash N M 2010 *Phys. Solid State* **52** 167
[81] Gorev M V, Bogdanov E V, Flerov I N, Voronov V N and Laptash N M 2010 *Ferroelectrics* **397** 76
[82] Gorev M V, Flerov I N, Bogdanov E V, Voronov V N and Laptash N M 2010 *Phys. Solid State* **52** 377
[83] Flerov I N, Gorev M V, Bogdanov E V and Laptash N M 2016 *Ferroelectrics* **500** 153
[84] Udovenko A A and Laptash N M 2008 *Acta Crystallogr. Sect. B: Struct. Sci.* **64** 527
[85] Dieterich W 1985 *J. Stat. Phys.* **39** 583
[86] Cazorla C and Errandonea D 2016 *Nano Lett.* **16** 3124
[87] Aznar A, Lloveras P, Romanini M, Barrio M, Tamarit J L, Cazorla C, Errandonea D, Mathur N D, Planes A, Moya X and Manosa L 2017 *Nat. Commun.* **8** 1851
[88] Li B, Kawakita Y, Ohira-Kawamura S, Sugahara T, Wang H, Wang J, Chen Y, Kawaguchi S I, Kawaguchi S, Ohara K, Li K, Yu D, Mole R, Hattori T, Kikuchi T, Yano S I, Zhang Z, Zhang Z, Ren W, Lin S, Sakata O, Nakajima K and Zhang Z 2019 *Nature* **567** 506
[89] Lloveras P, Aznar A, Barrio M, Negrier P, Popescu C, Planes A, Manosa L, Stern-Taulats E, Avramenko A, Mathur N D, Moya X and Tamarit J L 2019 *Nat. Commun.* **10** 1803
[90] Lloveras P, Stern-Taulats E, Barrio M, Tamarit J L, Crossley S, Li W, Pomjakushin V, Planes A, Manosa L, Mathur N D and Moya X 2015 *Nat. Commun.* **6** 8801
[91] Carvalho A M G, Imamura W, Usuda E O and Bom N M 2018 *Eur. Polym. J.* **99** 212
[92] Cong D, Xiong W, Planes A, Ren Y, Manosa L, Cao P, Nie Z, Sun X, Yang Z, Hong X and Wang Y 2019 *Phys. Rev. Lett.* **122** 255703
[93] Rodriguez C and Brown L C 1980 *Metall. Mater. Tran. A* **11** 147
[94] Ossmer H, Lambrecht F, Gultig M, Chluba C, Quandt E and Kohl M 2014 *Acta Mater.* **81** 9
[95] Xiao F, Jin M, Liu J and Jin X 2015 *Acta Mater.* **96** 292
[96] Wu R R, Bao L F, Hu F X, Wu H, Huang Q Z, Wang J, Dong X L, Li G N, Sun J R, Shen F R, Zhao T Y, Zheng X Q, Wang L C, Liu Y, Zuo W L, Zhao Y Y, Zhang M, Wang X C, Jin C Q, Rao G H, Han X F and Shen B G 2015 *Sci. Rep.* **5** 18027
[97] Samanta T, Lloveras P, Us Saleheen A, Lepkowski D L, Kramer E, Dubenko I, Adams P W, Young D P, Barrio M, Tamarit J L, Ali N and Stadler S 2018 *Appl. Phys. Lett.* **112** 021907
[98] Mañosa L, Stern-Taulats E, Planes A, Lloveras P, Barrio M, Tamarit J L, Emre B, Yüce S, Fabbrici S and Albertini F 2014 *Phys. Status Solidi B* **251** 2114
[99] Flerov I N, Kartashev A V, Gorev M V, Bogdanov E V, Mel'nikova S V, Molokeev M S, Pogoreltsev E I and Laptash N M 2016 *J. Fluor. Chem.* **183** 1